

D-Wave and Pair-Density-Wave Superconductivity in the Square-Lattice t - J Model

Feng Chen,¹ F. D. M. Haldane,² and D. N. Sheng¹

¹*Department of Physics and Astronomy, California State University, Northridge, California 91330, USA*

²*Department of Physics, Princeton University, Princeton NJ 08544, USA*

(Dated: November 28, 2023)

The Hubbard and closely related t - J models are exciting platforms for unconventional superconductivity. Through state-of-the-art density matrix renormalization group calculations using the grand canonical ensembles, we address open issues regarding the ground-state phase diagram of the extended t - J model on a square lattice in the parameter regime relevant to cuprate superconductors. On large 8-leg cylinders, we demonstrate that the pure t - J model with only nearest-neighbor hoppings and superexchange interactions, for a wide range of hole doping ($\delta = 0.1 - 0.2$), hosts an exotic SC state where the d-wave and unidirectional pair density wave SC co-exist with spin and charge bond orders. Furthermore, a small next nearest neighbor hopping t_2 suppresses the pair density wave and other co-existing orders, leading to a d-wave SC phase in both electron- and hole-doped cuprate model systems. We reveal a simple mechanism for SC in the t - J model, in which the nearest neighbor hopping plays an essential role in driving the formation of Cooper pairs with real-space sign oscillations balancing the competition between the kinetic and exchange energies. Our work validates the t - J model as a proper minimum model for describing fundamental physics of cuprate superconductors.

Introduction.— The mechanism of high-temperature superconductivity (SC) in cuprate compounds is one of the major challenges in condensed matter physics [1–3]. The emergence of superconductivity from doping the antiferromagnetic Mott insulating phase of cuprates suggests the square-lattice Hubbard model in the strong coupling regime and the closely related t - J model as the minimal models for its theoretical understandings [1–10]. On the analytical side, resonating valence bond (RVB) theory has presented a picture of developing unconventional SC from spin liquid background [1, 4, 7, 11–14]. New concepts such as spin-charge separation, spin liquid, electron fractionalization, and intertwined spin and charge orders have also been extensively explored and may play important roles in understanding doped Mott insulators [1, 4, 6, 8, 9, 15–21]. However, various analytical approximations are not controlled in identifying quantum phases of these strongly correlated systems. On the other hand, extensive numerical simulations in recent years have often identified the stripe phase in the ground states of the pure t - J and Hubbard models with only nearest-neighbor (NN) hoppings [22–34]. Meanwhile, there are also indications that the stripe phase has local pairing tendency [32, 33, 35] and is in strong competition with SC order [36–40]. Therefore, it is fundamentally important to re-examine if the pure t - J model can host SC ground state, and identify the physical reasons for its emergence or absence.

To provide a more realistic modeling of cuprate systems, the extended t - J and Hubbard models with both NN and next-nearest-neighbor (NNN) hoppings (t_1, t_2) have been extensively studied and the choice of the positive or negative t_2 corresponds to electron-doped or hole-doped cuprates with the Fermi surface topology consistent with experiments [32, 41–43]. Earlier numerical studies have found that positive t_2 enhances d -wave SC order whereas negative t_2 promotes the stripe phase and suppresses SC [44–46], or favors plaquette-type pairing in width-4 cylinders [26, 29, 47, 48] around the optimal hole doping. More recently, density matrix renormalization group (DMRG) [49] studies of the extended t - J model have reached a consensus on the presence of robust d -

wave SC on wider cylinders with the width L_y upto $L_y = 8$ for parameter regime $t_2/t_1 \gtrsim 0.1$, marking a significant step towards establishing d -wave SC for electron-doped cuprate model [32, 33, 40, 50] or doping spin liquid (or spin-liquid-like states) [51, 52]. However, numerical results on the hole-doped model ($t_2 < 0$) remain controversial. Previous DMRG studies reported the stripe formation and absence of SC in the ground state of the hole-doped t - J model [32, 33, 53], whereas latest DMRG simulations using larger bond dimensions have identified the melting of charge density wave (CDW) and emergence of weak SC as the system widens from $L_y = 6$ to 8 at 1/8 hole doping [40]. It remains challenging to fully understand the competition and interplay between CDW, magnetic order and SC, and reveal a unified mechanism for the emergence of SC in the family of t - J models.

In this article, we address open issues regarding the emergence of unconventional SC by studying the extended t - J model on a square lattice based on state-of-the-art DMRG simulations of grand canonical [32] systems up to $L_y = 8$. We establish a global phase diagram (Fig. 1(c)) where the d -wave SC order is prevalent over the entire parameter regime with the doping level $0.1 \leq \delta \leq 0.2$ and hopping ratio $-0.2 \leq t_2/t_1 \leq 0.3$. In particular, an exotic SC phase emerges in the pure t - J model ($t_2 = 0$) where isotropic d -wave SC coexists with period-2 unidirectional pair density wave (PDW) [54], spin bond order and weak charge order in real space. In the hole-doped t - J model with negative $t_2/t_1 \sim -0.1$, a SC-CDW phase appears with co-existing d -wave SC and CDW orders. A common uniform SC phase emerges at relatively larger magnitude $t_2/t_1 \sim \pm 0.2$, suggesting a symmetry between the electron- and hole-doped t - J models through suppressing competing orders. The universal emergence of SC in the extended t - J model is revealed to be driven by the frustrating NN hopping (t_1) that turns the pre-existing RVB pairs into coherent Cooper pairs upon doping. Our results validate the t - J model as the suitable minimal model for describing cuprate SC and provide benchmark results for future theoretical studies.

Model and Method.— We consider the square-lattice

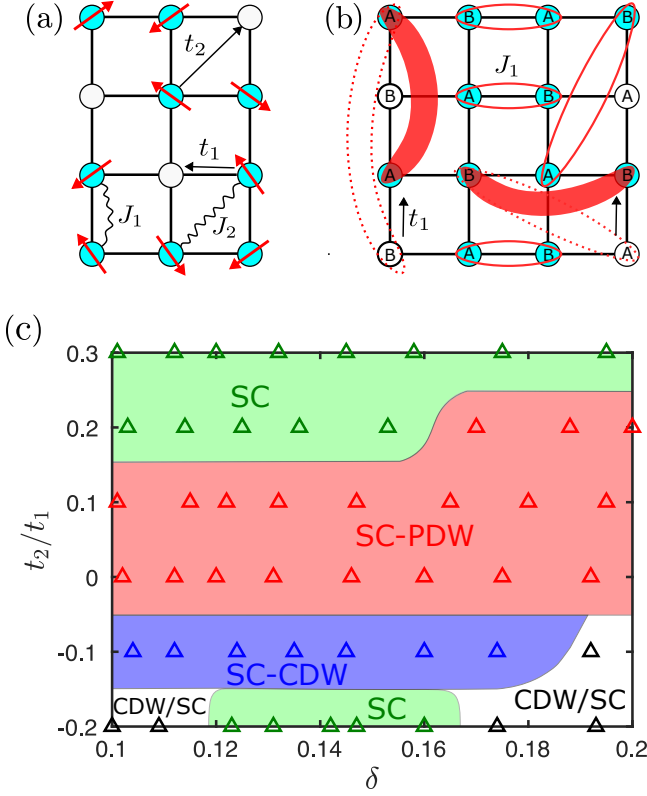


FIG. 1. (a) Illustration of the extended t - J model. (b) Illustration of the development of same-sublattice pairings (denoted by filled ovals) from opposite-sublattice ones (denoted by unfilled ovals) in the pure t - J model as a consequence of NN electron hopping. (c) Ground-state phase diagram under the variation of doping level δ and ratio t_2/t_1 . Three SC phases are found. The uniform d -wave superconducting phase is denoted by SC and the superconducting phase coexisting with period-2 PDW or weak CDW is denoted by SC-PDW or SC-CDW, respectively. The white region at the lower corners has strong competition between CDW and SC, which cannot be fully resolved with the currently accessible bond dimensions.

t_1 - t_2 - J_1 - J_2 model defined as

$$H = - \sum_{\{ij\}, \sigma} t_{ij} (\hat{c}_{i,\sigma}^\dagger \hat{c}_{j,\sigma} + \text{H.c.}) + \sum_{\{ij\}} J_{ij} (\hat{\mathbf{S}}_i \cdot \hat{\mathbf{S}}_j - \frac{1}{4} \hat{n}_i \hat{n}_j) - \mu \sum_i \hat{n}_i, \quad (1)$$

where $\hat{c}_{i\sigma}^\dagger$ and $\hat{c}_{i\sigma}$ are the creation and annihilation operators of the electron with spin σ ($\sigma = \pm 1/2$) at site $i = (x, y)$, $\hat{\mathbf{S}}_i$ is the spin-1/2 operator and $\hat{n}_i = \sum_\sigma \hat{c}_{i\sigma}^\dagger \hat{c}_{i\sigma}$ is the electron number operator. Double occupancy is prohibited. The electron hoppings t_{ij} and the spin exchange interactions J_{ij} are restricted to the NN (t_1 , J_1) and NNN (t_2 , J_2) terms. We consider a cylinder that is periodic along the circumferential (\hat{y}) direction and open along the axial (\hat{x}) direction with width L_y and length L_x respectively. The total number of sites is $N = L_x \times L_y$. We impose spin $SU(2)$ symmetry in the DMRG calculations [50, 55] and keep large bond dimensions up to $M = 15000$ (equivalent to about 45000 $U(1)$ states)

for accurate results, which gives a truncation error smaller or around 3.0×10^{-5} (see Supplemental Material [56] for more details). We consider the grand canonical ensemble where spontaneous symmetry breaking of the particle number conservation is allowed [32], and tune the average electron number by the chemical potential μ . The average doping level is defined as $\delta = 1 - \langle \sum_i \hat{n}_i \rangle / N$. Finally, we set $J_1 = 1$ as the energy unit and $t_1 = 3.0$, corresponding to a Hubbard model at $U/t_1 = 12$ [50, 51], and vary t_2 and J_2 together via the relation $J_2/J_1 = (t_2/t_1)^2$.

Phase Diagram— We focus on the regime of doping level $0.1 \leq \delta \leq 0.2$ and hopping ratio $-0.2 \leq t_2/t_1 \leq 0.3$ to obtain a phase diagram for $L_y = 8$ systems shown in Fig. 1(c). We identify three different SC phases: (1) A uniform d -wave SC phase appears at both $t_2/t_1 \gtrsim 0.15$ and $t_2/t_1 \lesssim -0.15$; (2) A SC phase coexisting with weak CDW order at $-0.15 \lesssim t_2/t_1 \lesssim -0.05$; (3) A nematic SC phase composed of uniform d -wave SC and a period-2 unidirectional PDW order with pairing momentum $\mathbf{k}_{\text{PDW}} = (0, \pi)$ for $-0.05 \lesssim t_2/t_1 \lesssim 0.15 - 0.25$ depending on doping levels. In the bottom corners of the phase diagram with $t_2/t_1 \sim -0.2$ and doping around $\delta \sim 0.11$ and 0.19 , there is also a possible CDW phase coexisting with weaker or vanishing SC order. The important role of the frustrating NN hopping t_1 is illustrated in Fig. 1(b), which allows the spin-singlet pairs in the same sublattice to develop. In the following, we will explore universal features of these SC phases and reveal the underlying mechanism for their emergence.

To identify the SC order, we examine the dominant spin-singlet NN pairing orders defined as:

$$\Delta_\alpha(x, y) = \langle \hat{c}_{(x,y),\uparrow} \hat{c}_{(x,y)+\hat{\alpha},\downarrow} - \hat{c}_{(x,y),\downarrow} \hat{c}_{(x,y)+\hat{\alpha},\uparrow} \rangle / \sqrt{2}, \quad (2)$$

where $\hat{\alpha} = \hat{x}$ or \hat{y} denotes the direction of the NN bond. In the grand canonical DMRG simulations [32, 56], the nonzero pairing orders detect the spontaneous $U(1)$ symmetry breaking: a low-energy “natural ground state” [57, 58] with symmetry breaking can be selected by DMRG algorithm to reduce long-range entanglement and Hilbert space fragmentation, so that the system effectively lowers its energy for finite bond dimensions. The “natural ground state” is a superposition of lower energy eigenstates (Anderson Tower of states) [57] for a system with the tendency of spontaneous symmetry breaking, and becomes near degenerate with the true ground state for large systems. Thus, the grand canonical simulation [32] for finite systems provides a natural way to detect SC and competing orders.

We first demonstrate the global emergence of SC as illustrated in Fig. 2. For four representative parameter points and a large system size $N = 50 \times 8$, we show NN SC pairing orders $\Delta_x(r)$ and $\Delta_y(r)$ with a magnitude proportional to the bond width in Fig. 2 (a1-a4). The opposite signs of the x - and y -bonds demonstrate a robust d -wave symmetry. Furthermore, Δ_x and Δ_y are nearly constant in the bulk regime for the uniform SC phase (Fig. 2 (b1,b4)), while there are noticeable oscillations of Δ_x along x -direction in the SC-CDW and SC-PDW phases (Fig. 2 (b2,b3)), indicating the coupling between CDW (Fig. 2 (c2,c3)) and the SC order Δ_x [19, 54]. In the SC-PDW phase of the pure t - J model, the most salient fea-

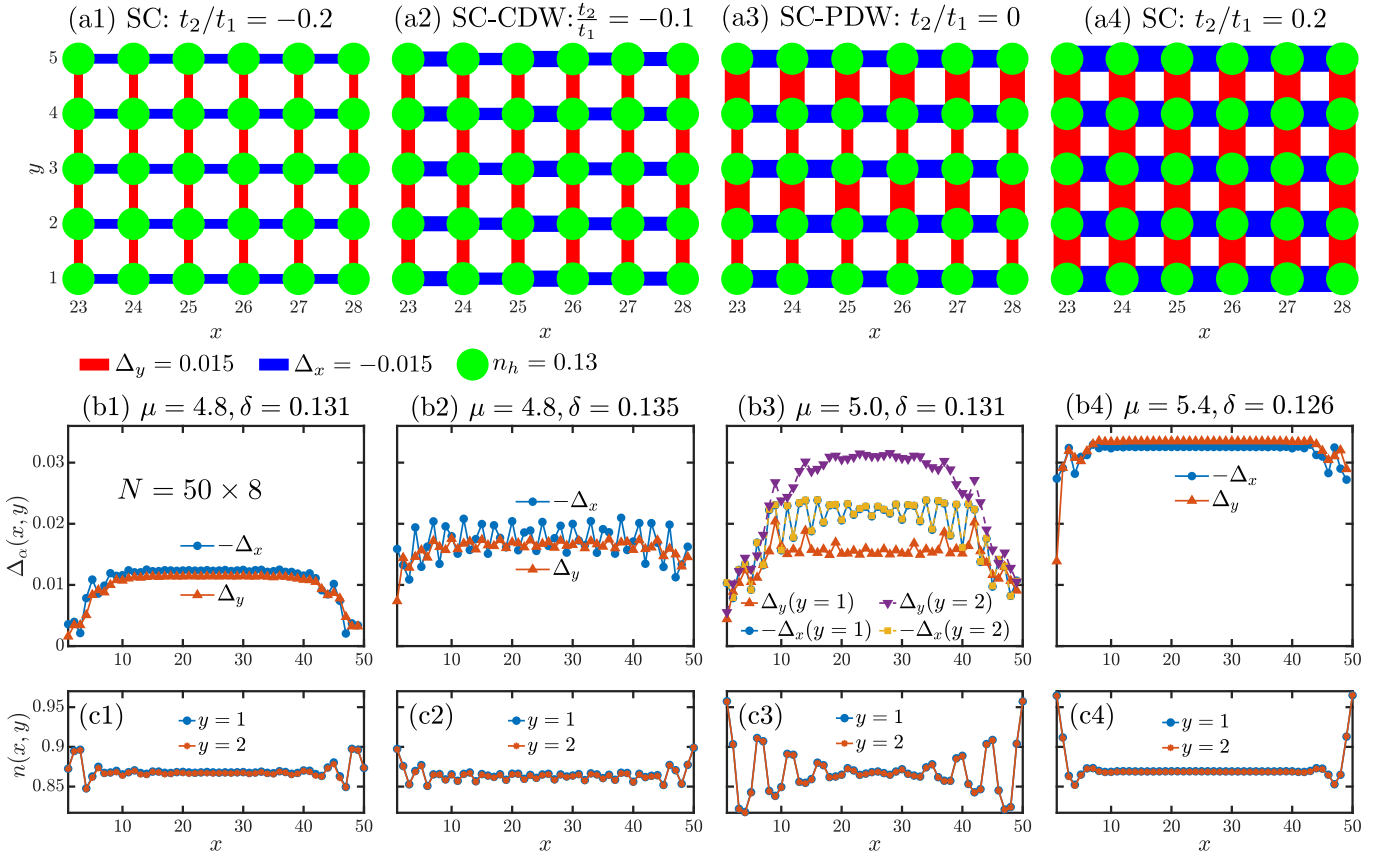


FIG. 2. The SC pairing orders and electron density profiles for four representative t_2/t_1 around 1/8 doping. (a) 2D plots for the NN pairing orders $\Delta_{\alpha=x,y}(\mathbf{r})$ and hole density $n_h(\mathbf{r}) = 1 - \langle \hat{n}_{\mathbf{r}} \rangle$ obtained at $M = 12000$. The bond thickness is proportional to the pairing amplitude and blue/red color denotes positive/negative sign respectively. The area of the green circle is proportional to the hole density $n_h(\mathbf{r})$ at each site. (b) The middle panels show the NN pairing orders $\Delta_{\alpha=x,y}$ along x -direction, which are uniform along \hat{y} for (b1, b2) and (b4) but oscillating along \hat{y} with a period of two lattice constants for Δ_y in (b3), i.e. in the pure t - J model. (c) The lower panels show the electron density profiles $n(x, y)$ for $y = 1, 2$.

ture is the oscillation of Δ_y with a period of 2 lattice spacings along y -direction as shown in Fig. 2 (a3,b3) corresponding to a PDW with a pair momentum $\mathbf{k}_{\text{PDW}} = (0, \pi)$. The electron density generally preserves translational invariance along y -direction. The electron density $n(x, y)$ for $y = 1, 2$ is shown in Fig. 2 (c1-c4). We identify a very uniform electron density $n(x, y)$ for the SC phase at $t_2/t_1 = \pm 0.2$ (see Fig. 2 (c1, c4)), and a very weak stripe pattern for the SC-CDW phase at $t_2/t_1 = -0.1$ along x direction. Interestingly, for the pure t - J model, the electron density shows stripe-like patterns along x -direction near the open boundaries (see Fig. 2 (c3)) and becomes flattened in the center of the system. Full nature of the SC-PDW phase will be presented below (see Fig. 4).

Overall, the SC order becomes stronger as t_2 gets more positive, and both positive and negative t_2 of large enough magnitudes ($|t_2/t_1| \gtrsim 0.15$) suppress CDW and PDW, resulting in a uniform d-wave SC phase. The uniform SC phase at $t_2/t_1 = 0.2 - 0.3$ identified here is consistent with earlier results from either grand canonical [32] or canonical DMRG studies [40, 50], further establishing the robust SC phase in the electron-doped t - J model. More significantly, we unify the hole- and electron-doped t - J models by establishing their

common uniform SC phase.

Uniform SC Phase and Competing Stripe Order in the Hole Doped t - J Model—A CDW in the stripe form was identified either as the ground state [32] or as a weak order co-existing with power-law SC correlations [40] for the hole-doped t - J model. Here we demonstrate how SC orders emerge through suppressing the stripe order in large 8-leg systems. Fig. 3 shows the charge densities, pairing orders $\Delta_{x,y}$ and pairing correlations $P_{yy}(r) = \langle \hat{\Delta}_y(x_0, y_0) \hat{\Delta}_y(x_0 + r, y_0) \rangle$ for systems at $t_2/t_1 = -0.2$ and $\mu = 4.8$, corresponding to an average doping $\delta \sim 0.13$. In Fig. 3(a1) for $N = 32 \times 8$, the CDW order is quite robust until M reaches the large value of $M = 15000$, where the CDW pattern is substantially weakened. The SC order Δ_x and Δ_y gradually develop from nearly vanishing to being notably strong when M is increased from 8000 to 15000 as shown in Fig. 3(b1). Along with the suppression of CDW order at $M = 15000$, we also see a drop of electron density (Fig. 3(a1)) as more holes are attracted into the system at fixed μ due to the much reduced (more negative) hopping energy (kinetic energy) [59]. Thus the melting of the CDW and the emergence of the SC are driven by the optimization of the kinetic energy [60]. Consistently, the pairing correla-

tion $P_{yy}(r)$ in Fig. 3(c1) also increases with M and exhibits a robust quasi-long-range SC order at $M = 15000$. Physically speaking, the CDW order is more classical and is the optimal low-energy state when the bond dimension is relatively small. Upon increasing the bond dimension, the more entangled state such as a coherent SC state is developed to effectively lower the total energy by balancing the kinetic and potential energies.

In a longer system with $N = 50 \times 8$, the SC orders Δ_x and Δ_y in Fig. 3(b2) are already quite robust at $M = 8000$ and are nearly independent of the bond dimension for $M = 8000 - 15000$, indicating a more robust SC phase for larger systems [56]. The SC order is weaker at the boundary but grows rapidly into the bulk (Fig. 3(b2)), whereas the charge modulations only appear around the system boundaries (Fig. 3(a2)). The uniform SC order and electron density in the bulk mark a uniform SC phase. Meanwhile, the pairing correlation in Fig. 3(c2) exhibits a power-law decay with a small power exponent[56], further supporting a robust SC phase.

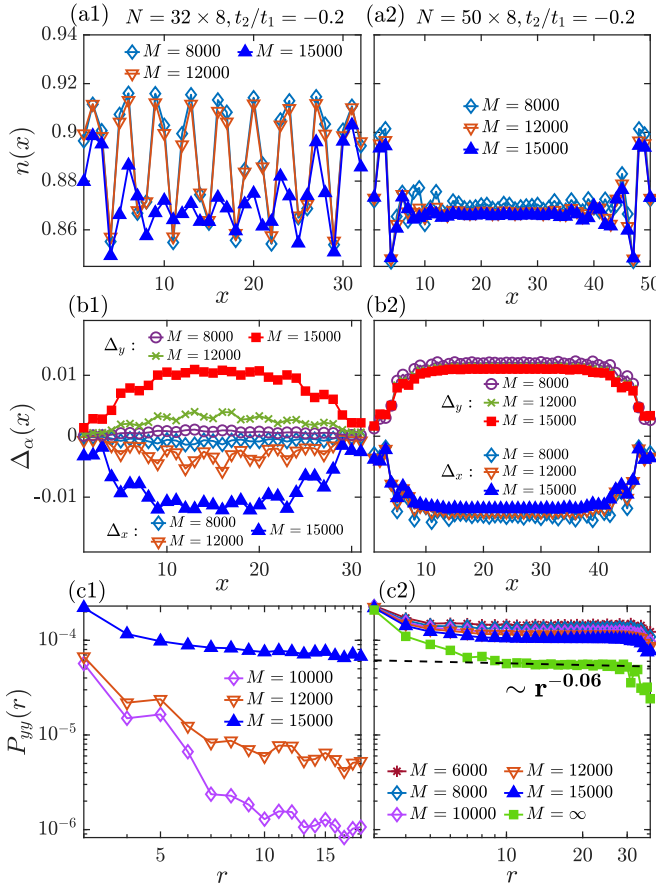


FIG. 3. The SC phase for the hole-doped t - J model with $t_2/t_1 = -0.2$ and $\mu = 4.8$. (a) Electron density profiles, (b) pairing orders and (c) y -bond pairing correlations $P_{yy}(r)$ at different bond dimensions for system sizes $N = 32 \times 8$ (left panels) and $N = 50 \times 8$ (right panels). The pairing correlations in (c2) are extrapolated to infinite M through second-order polynomial extrapolation, and the extrapolated data in the bulk can be fitted by a power-law decay with an exponent of $K_{sc} \sim 0.06$.

Exotic Co-Existing D-wave, Pair Density Wave Superconductivity, and Spin Bond Order for the Pure t - J Model.— Now we focus on the pure t - J model with $t_2 = J_2 = 0$. The pairing order Δ_y has a double unit cell along y -direction, and its average $\bar{\Delta}_y(x) = [\Delta_y(x, y = 2) + \Delta_y(x, y = 1)]/2$ has similar magnitude as Δ_x (Fig. 2 (b3)), forming the d-wave SC component $\bar{\Delta}_y(x) \sim 0.02$ after extrapolation to the infinite M limit as shown in Fig. 4(a). The PDW order of the SC-PDW phase is obtained by subtracting the d-wave background from the local SC order: $\Delta_y^{\text{pdw}}(x, y) = [\Delta_y(x, y) - \bar{\Delta}_y(x)]$, which has the following y -dependence:

$$\Delta_y^{\text{pdw}}(x, y) = (-1)^y \Delta_y^{\text{P}}(x), \quad (3)$$

indicating a unidirectional PDW with Cooper-pair momentum $\mathbf{k}_{\text{PDW}} = (0, \pi)$. The magnitude of the PDW order $\Delta_y^{\text{P}}(x)$ drops slightly with the increase of M and is extrapolated to $\Delta_y^{\text{P}} \approx 0.004$ as shown in Fig. 4(b). We illustrate the pattern of the PDW order $\Delta_y^{\text{pdw}}(x, y)$ in real space in Fig. 4(c), which is coupled with a spin-bond order $\langle \hat{S}_{x,y} \cdot \hat{S}_{x,y+1} \rangle$ with the same strong-weak unit-2 pattern as shown in Fig. 4(d). The SC-PDW phase also shows a weaker charge bond order[56]. To the best of our knowledge, such a PDW order has only been identified in more complex models, e.g. the three-band cuprate models [61–63], although it is highly desired and explored in phenomenological and mean-field studies of cuprate systems [25, 54, 64, 65].

Longer-Distance Cooper Pairs— We now explore the nature of the SC phases through imaging the real space distribution of the Cooper pairs. We define the longer-distance pairing orders $\hat{\Delta}(\mathbf{r}) \equiv \hat{\Delta}(x, y) = \langle \hat{c}_{(x_0, y_0), \uparrow} \hat{c}_{(x_0+x, y_0+y), \downarrow} - \hat{c}_{(x_0, y_0), \downarrow} \hat{c}_{(x_0+x, y_0+y), \uparrow} \rangle / \sqrt{2}$ between two points at positions (x_0, y_0) and (x_0+x, y_0+y) , which are shown in Fig. 5 as circles whose areas are proportional to their magnitudes and whose colors denote their signs. While the NN pairing orders follow a d-wave symmetry for all SC phases, an additional small s -wave component can be identified by the same sign and magnitude of the four NNN pairings at $t_2/t_1 = \pm 0.2$ as shown in Fig. 5(a,c). The longer-distance pairing order shows sign oscillations in real space and decays with the pairing separation. The length scale for its sign to repeat along \hat{x} -direction is identified to be $l_s = 5, 6, 3$, for $t_2/t_1 = -0.2, 0, 0.2$, respectively. Furthermore, the Cooper pairs at $t_2/t_1 = -0.2$ and 0 are extended into longer distances than that at $t_2/t_1 = 0.2$.

A common feature of all these SC states is the development of pairings between the same sublattices at intermediate distances comparable to l_s , indicating that such Cooper pairs gain kinetic energy through NN hoppings. Starting from the pure t - J model, the pre-existing long-range RVB pairs at half-filling are formed between opposite sublattices [13], following the Marshall sign rule [66] and supporting a long-range AFM order. Upon hole doping, as illustrated in Fig. 1(b), the NN electron hopping will bring RVB pairs between opposite sublattices into the same sublattice, breaking the Marshall sign rule and frustrating the AFM order. Therefore, the NN electron hopping is a key driving force in turning the pre-existing RVB pairs due to the NN spin exchange interactions

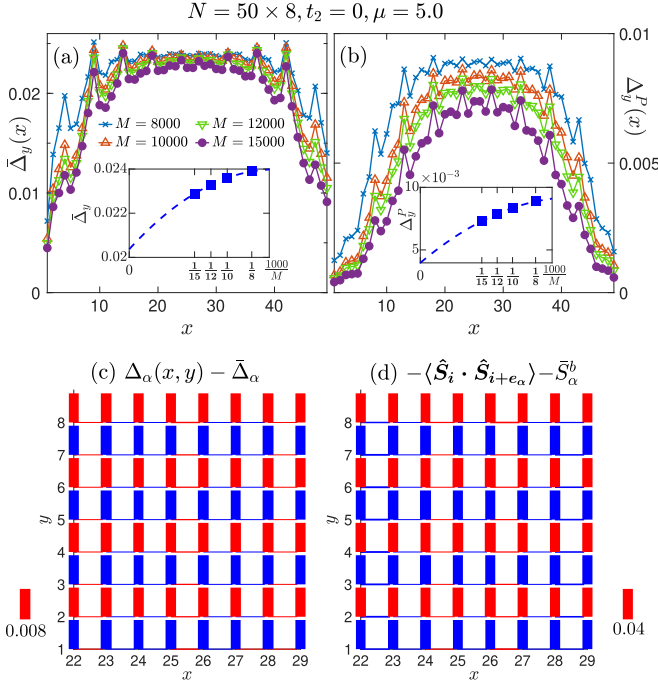


FIG. 4. The coexisting d-wave SC, PDW and spin bond orders in the SC-PDW phase for $t_2 = 0, \mu = 5.0$ and $N = 50 \times 8$. (a) The average y -bond SC pairing of the first and second legs $\bar{\Delta}_y(x) \equiv [\Delta_y(x, y=2) + \Delta_y(x, y=1)]/2$. The inset shows the second-polynomial extrapolation of the bulk $\bar{\Delta}_y$ (averaged over middle 10 sites) versus $1/M$: $\bar{\Delta}_y(M = \infty) = 0.02$. (b) The magnitude of PDW $\Delta_y^p(x)$ defined in Eq. 3. The bulk value after extrapolation is $\Delta_y^p(M = \infty) = 0.004$. (c) Illustration of the unidirectional PDW with momentum $\mathbf{k}_{\text{PDW}} = (0, \pi)$. The x - and y -bond mean values $\bar{\Delta}_x = -0.0223$ and $\bar{\Delta}_y = 0.0233$ are subtracted from Δ_x and Δ_y respectively. (d) Nearest-neighbor spin bond orders $-\langle \hat{\mathbf{S}}_i \cdot \hat{\mathbf{S}}_{i+e_\alpha} \rangle - \bar{S}_\alpha^b$ in the central region, subtracting the anisotropic x - and y -bond mean values $\bar{S}_x^b = 0.1852$ and $\bar{S}_y^b = 0.2215$. The red/blue color represents positive/negative value respectively and the bond widths are proportional to the magnitudes of the quantity represented. A reference bond and its magnitude is put beside each lattice plot. (c) and (d) are obtained under $M = 12000$.

into coherent SC Cooper pairs [9]. For the pure t - J model, the longer-distance Cooper pairs are developed through breaking the d-wave symmetry of the NN pair order by inducing an additional unidirectional PDW order intertwining with spin and charge bond orders. After pinning down the SC for the pure t - J model, it becomes clear what is the role of NNN hoppings: they help longer-distance Cooper pairs to develop in more symmetric ways and suppress the nematicity or PDW tendency of the pure t - J model. Furthermore, the distinct signs of the NNN hoppings for hole- and electron-doped t - J models results in different length scale l_s for sign oscillation of $\tilde{\Delta}(\mathbf{r})$ and larger l_s on the hole-doped side makes the SC harder to emerge until the system reaches $L_y = 8$ [33, 40]. For the electron-doped t - J model, the SC orders also grow stronger as the system widens from $L_y = 6$ to 8 [56]. Our results demonstrate a unified picture for understanding the global phase diagram of the t - J model, driven by NN hop-

ping in addition to the spin exchange interaction. Their cooperative interplay [9] is the key mechanism for the general emergence of SC around optimal doping in these systems.

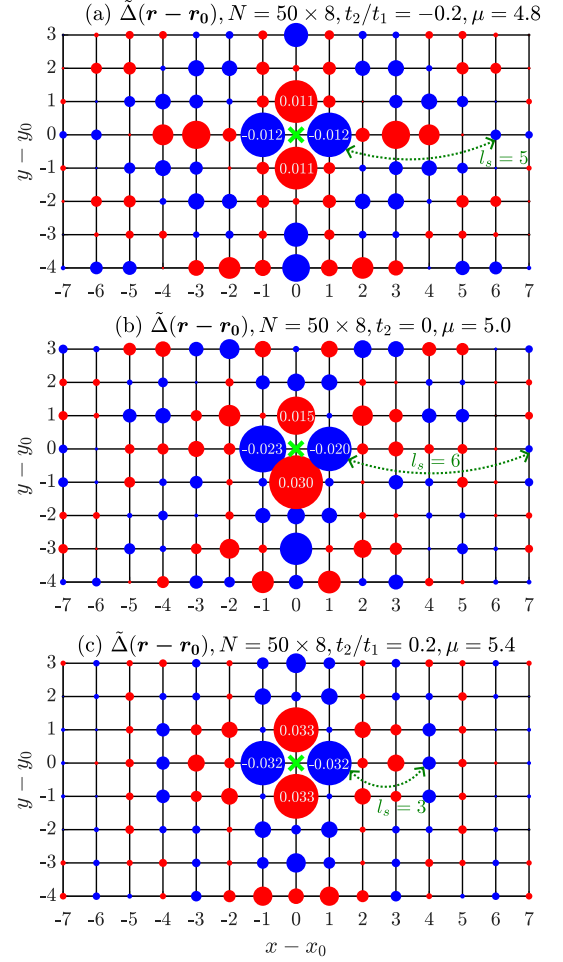


FIG. 5. Long-distance pairings $\tilde{\Delta}(\mathbf{r} - \mathbf{r}_0)$ imaging real space Cooper pairs. The reference point $(x_0, y_0) = (25, 5)$ for (a-c) is marked by a green cross. The areas of the circles are proportional to the magnitudes of $\tilde{\Delta}(\mathbf{r} - \mathbf{r}_0)$ and the red/green color denotes its positive/negative sign. The associated values of nearest-neighbor pairings are given in the figures. Data are obtained under $M = 15000$.

Exponentially Decaying Spin and Charge Correlations— Now we compare length scales of the Cooper pair wave function, charge and spin correlations for the pure t - J model. As shown in Fig. 6(a), the longer-distance pairing order $\tilde{\Delta}(\mathbf{r})$ decreases exponentially with the distance r between two paired electrons, characterized by an effective Cooper pair correlation length or size $\xi_P = 3.74$. Similar small length scales $\xi_P = 2.44$ and 2.01 are also found for $t_2/t_1 = \mp 0.2$, respectively [56]. The relative magnitudes of ξ_P for different t_2/t_1 are consistent with those of l_s , showing the largest Cooper pair size at $t_2 = 0$. Meanwhile, the single-particle Green's function $G(r) = \langle \sum_\sigma \hat{c}_\sigma^\dagger(x, y) \hat{c}_\sigma(x + r, y) \rangle$, spin correlation $S(r) = \langle \hat{\mathbf{S}}(x, y) \cdot \hat{\mathbf{S}}(x + r, y) \rangle$ and charge density correlation $D(r) = \langle \hat{n}(x, y) \hat{n}(x + r, y) \rangle - \langle \hat{n}(x, y) \rangle \langle \hat{n}(x + r, y) \rangle$ can all be described by exponential decays with very short correlation

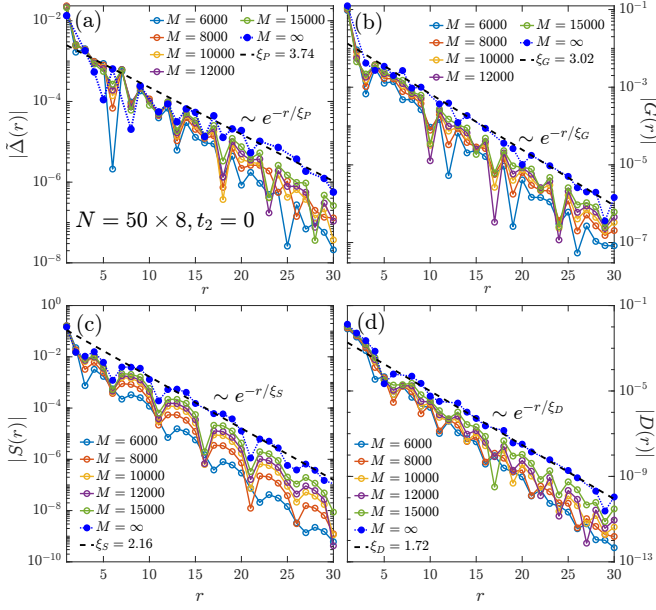


FIG. 6. Cooper pair and spin/charge correlation lengths for the SC-PDW phase at $t_2/t_1 = 0$ and $\mu = 5.0$. (a) Non-local pairing $\hat{\Delta}(r)$ versus pair-distance r along x -direction for different bond dimension M s and its extrapolation to infinite M , giving an exponential decay with a correlation length $\xi_P = 3.74$ representing the average Cooper-pair size. (b-d) are similar plots for single-particle Green's function, spin and charge-density correlations, with fitted correlation lengths $\xi_G = 3.02$, $\xi_S = 2.16$ and $\xi_D = 1.72$.

lengths comparable to the Cooper pair size ξ_P (see Fig. 6(b-d)). The short-range spin and charge correlations are generally observed for all SC phases (see SM [56] Fig. S4), similar to the previous identified SC phase by doping the spin liquid or spin-liquid like states [51, 52]. These results indicate a simple kinetic-energy-driven mechanism for the emergence of spin liquid background: the NN hopping frustrates the AFM order and turns the spin background into a short-range spin liquid.

Summary and Outlook— Through state-of-the-art DMRG simulations combining grand canonical ensembles [32] with a rigorous finite bond dimension analysis, we establish a global quantum phase diagram and unveil the universal emergence of SC in the general t - J model around the optimal hole doping ($0.1 \leq \delta \leq 0.2$). Of particular interest is the pure t - J model, whose ground state is determined to be an exotic phase with coexisting d-wave SC, unidirectional PDW, spin bond order and weaker charge bond order. Our results support the pure t - J model as a minimal model for understanding uncon-

ventional SC in doped Mott insulators, a conclusion of great importance as a d-wave SC ground state has never been observed before in unbiased numerical simulations of the pure t - J model [32, 40]. Beyond the pure t - J model, we establish the uniform SC phase in both hole- and electron-doped regimes, where SC grows stronger or only emerges for wider systems ($L_y = 8$), suggesting SC in the 2D limit. The necessity of large bond dimensions and system sizes for the hole-doped SC phase to emerge is due to the stronger competition between kinetic and exchange energies in the presence of additional Berry phase of the negative NNN hopping [33], which leads to spatially larger Cooper pairs with larger length scale of sign oscillations (Fig. 5). A key driving force for the SC in the t - J model, besides the NN spin exchange interaction [4], is identified here as the frustrating NN hopping that transforms the pre-existing long-range RVB pairs in the AFM spin background into finite-range phase-coherent SC pairs upon increasing doping.

Given the observation of prevalent SC in the extended t - J model in this work, it is natural to ask if one can also establish a unified mechanism for the unconventional SC in the one-band Hubbard model [29–31, 34, 67–69] for cuprates. Ground-state SC has been identified in the Hubbard model with NNN hopping using both DMRG and auxiliary field quantum Monte Carlo methods in the grand canonical finite-size systems in the presence of a global pairing field [68]. While their results demonstrate the emergence of SC in both electron- and hole-doped regimes, consistent with our results, the detailed nature of Cooper pairs is not known there, and thus we believe our work will stimulate more extensive exploration of the extended Hubbard model to identify a unified mechanism of unconventional SC. Furthermore, it would be interesting to reexamine the pure Hubbard model ($t_2 = 0$) to understand if the absence of SC in numerical studies presented so far [31, 34, 68] is related to finite-size and/or low entanglement effects (favoring conventional charge or spin orders), which will be addressed in the future.

We thank Leon Balents, S. S. Gong, Xin Lu, H. C. Jiang, Shengtao Jiang, S. A. Kivelson, S. R. White, Z. Y. Weng, and Wei Zhu for stimulating discussions. This work was supported by the U.S. Department of Energy, Office of Basic Energy Sciences under Grant No. DE-FG02-06ER46305 (FC, DNS) for computational study, and National Science Foundation (NSF) Princeton Center for Complex Materials, a Materials Research Science and Engineering Center DMR-2011750 (FDMH). D.N.S. also acknowledges partial support from NSF Partnership in Research and Education in Materials DMR-1828019 for her travel to Princeton.

- [1] P. A. Lee, N. Nagaosa, and X.-G. Wen, *Rev. Mod. Phys.* **78**, 17 (2006), publisher: American Physical Society.
- [2] B. Keimer, S. A. Kivelson, M. R. Norman, S. Uchida, and J. Zaanen, *Nature* **518**, 179 (2015).
- [3] C. Proust and L. Taillefer, *Annual Review of Condensed Matter Physics* **10**, 409 (2019).
- [4] P. W. Anderson, *Science* **235**, 1196 (1987), publisher: American Association for the Advancement of Science.

- [5] F. C. Zhang and T. M. Rice, *Phys. Rev. B* **37**, 3759 (1988).
- [6] D. S. Rokhsar and S. A. Kivelson, *Phys. Rev. Lett.* **61**, 2376 (1988).
- [7] P. W. Anderson, P. A. Lee, M. Randeria, T. M. Rice, N. Trivedi, and F. C. Zhang, *Journal of Physics: Condensed Matter* **16**, R755 (2004).

- [8] S. Sachdev, *Rev. Mod. Phys.* **75**, 913 (2003).
- [9] Z. Y. Weng, D. N. Sheng, Y.-C. Chen, and C. S. Ting, *Phys. Rev. B* **55**, 3894 (1997), publisher: American Physical Society.
- [10] M. Ogata and H. Fukuyama, *Rep. Prog. Phys.* **71**, 036501 (2008).
- [11] P. W. Anderson, G. Baskaran, Z. Zou, and T. Hsu, *Phys. Rev. Lett.* **58**, 2790 (1987), publisher: American Physical Society.
- [12] S. A. Kivelson, D. S. Rokhsar, and J. P. Sethna, *Phys. Rev. B* **35**, 8865 (1987), publisher: American Physical Society.
- [13] S. Liang, B. Douçot, and P. W. Anderson, *Phys. Rev. Lett.* **61**, 365 (1988).
- [14] D. J. Scalapino, *Rev. Mod. Phys.* **84**, 1383 (2012), publisher: American Physical Society.
- [15] X. G. Wen, *Phys. Rev. B* **44**, 2664 (1991).
- [16] T. Senthil and M. P. A. Fisher, *Phys. Rev. B* **62**, 7850 (2000).
- [17] R. K. Kaul, Y. B. Kim, S. Sachdev, and T. Senthil, *Nature Physics* **4**, 28 (2008).
- [18] L. Balents and S. Sachdev, *Annals of Physics* **322**, 2635–2664 (2007).
- [19] E. Fradkin, S. A. Kivelson, and J. M. Tranquada, *Rev. Mod. Phys.* **87**, 457 (2015), publisher: American Physical Society.
- [20] Z.-Y. Weng, *New J. Phys.* **13**, 103039 (2011), publisher: IOP Publishing.
- [21] H.-C. Jiang and S. A. Kivelson, *Proceedings of the National Academy of Sciences* **119**, e2109406119 (2022), publisher: Proceedings of the National Academy of Sciences.
- [22] S. R. White and D. J. Scalapino, *Phys. Rev. Lett.* **80**, 1272 (1998), publisher: American Physical Society.
- [23] S. R. White and D. J. Scalapino, *Phys. Rev. Lett.* **91**, 136403 (2003).
- [24] G. Hager, G. Wellein, E. Jeckelmann, and H. Fehske, *Phys. Rev. B* **71**, 075108 (2005).
- [25] E. Berg, E. Fradkin, S. A. Kivelson, and J. M. Tranquada, *New Journal of Physics* **11**, 115004 (2009).
- [26] J. F. Dodaro, H.-C. Jiang, and S. A. Kivelson, *Phys. Rev. B* **95**, 155116 (2017), publisher: American Physical Society.
- [27] B.-X. Zheng, C.-M. Chung, P. Corboz, G. Ehlers, M.-P. Qin, R. M. Noack, H. Shi, S. R. White, S. Zhang, and G. K.-L. Chan, *Science* **358**, 1155 (2017).
- [28] K. Ido, T. Ohgoe, and M. Imada, *Phys. Rev. B* **97**, 045138 (2018).
- [29] H.-C. Jiang and T. P. Devereaux, *Science* **365**, 1424 (2019).
- [30] B. Ponsioen, S. S. Chung, and P. Corboz, *Phys. Rev. B* **100**, 195141 (2019).
- [31] Simons Collaboration on the Many-Electron Problem, M. Qin, C.-M. Chung, H. Shi, E. Vitali, C. Hubig, U. Schollwöck, S. R. White, and S. Zhang, *Phys. Rev. X* **10**, 031016 (2020), publisher: American Physical Society.
- [32] S. Jiang, D. J. Scalapino, and S. R. White, *Proceedings of the National Academy of Sciences* **118**, e2109978118 (2021), publisher: Proceedings of the National Academy of Sciences.
- [33] X. Lu, J.-X. Zhang, S.-S. Gong, D. N. Sheng, and Z.-Y. Weng, (2023), [arXiv:2303.13498 \[cond-mat.str-el\]](https://arxiv.org/abs/2303.13498).
- [34] Y.-F. Jiang, T. P. Devereaux, and H.-C. Jiang, (2023), [arXiv:2303.15541 \[cond-mat\]](https://arxiv.org/abs/2303.15541).
- [35] A. Wietek, *Phys. Rev. Lett.* **129**, 177001 (2022).
- [36] P. Corboz, T. Rice, and M. Troyer, *Phys. Rev. Lett.* **113**, 046402 (2014), publisher: American Physical Society.
- [37] M. Raczkowski, M. Capello, D. Poilblanc, R. Frésard, and A. M. Oleś, *Phys. Rev. B* **76**, 140505 (2007).
- [38] K.-Y. Yang, W. Q. Chen, T. M. Rice, M. Sigrist, and F.-C. Zhang, *New J. Phys.* **11**, 055053 (2009).
- [39] J.-W. Li, B. Bruognolo, A. Weichselbaum, and J. von Delft, *Phys. Rev. B* **103**, 075127 (2021), publisher: American Physical Society.
- [40] X. Lu, F. Chen, W. Zhu, D. N. Sheng, and S.-S. Gong, (2023), [arXiv:2304.03963 \[cond-mat.str-el\]](https://arxiv.org/abs/2304.03963).
- [41] A. Damascelli, Z. Hussain, and Z.-X. Shen, *Rev. Mod. Phys.* **75**, 473 (2003).
- [42] A. Nazarenko, K. J. E. Vos, S. Haas, E. Dagotto, and R. J. Gooding, *Phys. Rev. B* **51**, 8676 (1995).
- [43] C. Kim, P. J. White, Z.-X. Shen, T. Tohyama, Y. Shibata, S. Maekawa, B. O. Wells, Y. J. Kim, R. J. Birgeneau, and M. A. Kastner, *Phys. Rev. Lett.* **80**, 4245 (1998).
- [44] S. R. White and D. J. Scalapino, *Phys. Rev. B* **60**, R753 (1999), publisher: American Physical Society.
- [45] G. B. Martins, J. C. Xavier, L. Arrachea, and E. Dagotto, *Phys. Rev. B* **64**, 180513 (2001), publisher: American Physical Society.
- [46] A. Himeda, T. Kato, and M. Ogata, *Phys. Rev. Lett.* **88**, 117001 (2002), publisher: American Physical Society.
- [47] The Simons Collaboration on the Many-Electron Problem, C.-M. Chung, M. Qin, S. Zhang, U. Schollwöck, and S. R. White, *Phys. Rev. B* **102**, 041106 (2020), publisher: American Physical Society.
- [48] Y.-F. Jiang, J. Zaanen, T. P. Devereaux, and H.-C. Jiang, *Phys. Rev. Res.* **2**, 033073 (2020), publisher: American Physical Society.
- [49] S. R. White, *Phys. Rev. Lett.* **69**, 2863 (1992), publisher: American Physical Society.
- [50] S. Gong, W. Zhu, and D. Sheng, *Phys. Rev. Lett.* **127**, 097003 (2021), publisher: American Physical Society.
- [51] H.-C. Jiang and S. A. Kivelson, *Phys. Rev. Lett.* **127**, 097002 (2021), publisher: American Physical Society.
- [52] H.-C. Jiang, S. A. Kivelson, and D.-H. Lee, *Phys. Rev. B* **108**, 054505 (2023), publisher: American Physical Society.
- [53] S. Jiang, D. J. Scalapino, and S. R. White, *Phys. Rev. B* **106**, 174507 (2022).
- [54] D. F. Agterberg, J. S. Davis, S. D. Edkins, E. Fradkin, D. J. Van Harlingen, S. A. Kivelson, P. A. Lee, L. Radzihovsky, J. M. Tranquada, and Y. Wang, *Annual Review of Condensed Matter Physics* **11**, 231 (2020), eprint: <https://doi.org/10.1146/annurev-conmatphys-031119-050711>.
- [55] I. P. McCulloch and M. Gulácsi, *EPL* **57**, 852 (2002), publisher: IOP Publishing.
- [56] See Supplementary Materials for more supporting data.
- [57] H. Tasaki, *J Stat Phys* **174**, 735 (2019).
- [58] H.-C. Jiang, Z. Wang, and L. Balents, *Nature Physics* **8**, 902 (2012).
- [59] The chemical potential term $-\mu \sum_i \hat{n}_i$ and the superexchange term $\sum_{\langle ij \rangle} J_{ij} (\hat{\mathbf{S}}_i \cdot \hat{\mathbf{S}}_j - \frac{1}{4} \hat{n}_i \hat{n}_j)$ both increase as the electron occupation is lowered.
- [60] J.-Y. Zhao, S. A. Chen, H.-K. Zhang, and Z.-Y. Weng, *Phys. Rev. X* **12**, 011062 (2022).
- [61] H.-C. Jiang and T. P. Devereaux, (2023), [arXiv:2309.11786 \[cond-mat.str-el\]](https://arxiv.org/abs/2309.11786).
- [62] H.-C. Jiang, *Phys. Rev. B* **107**, 214504 (2023).
- [63] B. Ponsioen, S. S. Chung, and P. Corboz, (2023), [arXiv:2306.12910 \[cond-mat.str-el\]](https://arxiv.org/abs/2306.12910).
- [64] P. Choubey, S. H. Joo, K. Fujita, Z. Du, S. D. Edkins, M. H. Hamidian, H. Eisaki, S. Uchida, A. P. Mackenzie, J. Lee, J. C. S. Davis, and P. J. Hirschfeld, *Proceedings of the National Academy of Sciences* **117**, 14805 (2020), publisher: Proceedings of the National Academy of Sciences.
- [65] W.-L. Tu and T.-K. Lee, *Sci Rep* **9**, 1719 (2019), number: 1 Publisher: Nature Publishing Group.
- [66] W. Marshall, *Proceedings of the Royal Society of London. Se-*

- ries A. Mathematical and Physical Sciences **232**, 48 (1955).
- [67] M. Qin, T. Schäfer, S. Andergassen, P. Corboz, and E. Gull, [Annual Review of Condensed Matter Physics](#) **13**, 275 (2022), eprint: <https://doi.org/10.1146/annurev-conmatphys-090921-033948>.
 - [68] H. Xu, C.-M. Chung, M. Qin, U. Schollwöck, S. R. White, and S. Zhang, (2023), [arXiv:2303.08376 \[cond-mat.supr-con\]](#).
 - [69] C. Zhang, J.-W. Li, and J. von Delft, (2023), [arXiv:2307.14835 \[cond-mat\]](#).
 - [70] M. Fishman, S. R. White, and E. M. Stoudenmire, [SciPost Phys. Codebases](#) , 4 (2022).

Supplemental Materials

In the Supplemental Materials, we provide additional numerical results to support the conclusions made in the main text. In Sec. A we show evolution of pairing orders and pair-pair correlation functions with the bond dimension for six- and eight-leg cylinders by canonical and grand canonical simulations with spin $SU(2)$ or $U(1)$ symmetries, establishing the reliability of our simulations. In Sec. B, we provide an example of the finite bond dimension scaling of the ground state energy to demonstrate the numerical convergence of DMRG results. Furthermore, we demonstrate the equivalence of spin $SU(2)$ and $U(1)$ simulations in capturing long-range SC pairing orders. In Sec. C, we show pairing correlations of the SC-PDW phase and demonstrate the weak charge-bond order. In Sec. D, we show the exponentially decaying long-range pairing orders, single-particle Green's function, spin and density correlations for $t_2/t_1 = \pm 0.2$.

Appendix A: Evolution of SC order and pairing correlations in DMRG Simulations

As discussed in the main text, the DMRG simulations allow spontaneous symmetry breaking [32], through targeting the “natural ground state” as a superposition of low-energy states (Anderson Tower of states) [57], which becomes near degenerate with the true ground state for large systems. In this section, we provide systematical comparisons between canonical and grand canonical DMRG results with spin $SU(2)$ or $U(1)$ symmetries. In Fig. S1(a), we show how the SC order evolves with the bond dimension M (or m) in the grand canonical finite-size $SU(2)$ (or $U(1)$) DMRG simulations at a fixed chemical potential $\mu = 5.4$ and $t_2/t_1 = 0.2$. ITensor library [70] has been used for the $U(1)$ simulations. On the six-leg systems, the SC order sharply increases between $m = 1000$ and 3000 . After reaching a maximum value, Δ_y remains strong with the increase of the bond dimension, and such a behavior becomes more robust for a larger system with $N = 50 \times 8$, as demonstrated by the larger maximum value of Δ_y and slower decay with M . In the whole range of bond dimensions, the obtained Δ_y and ground state energy for $SU(2)$ and $U(1)$ DMRGs agree with each other as long as we take $M \sim m/3$, demonstrating the higher efficiency of $SU(2)$ simulations. The development of SC order, its plateau behaviour and increased stability with the growing of system sizes reveal the robustness of the SC state in the thermodynamic limit. This is similar to the detection of the Néel order in the thermodynamic limit [32] by the finite-size spin- $U(1)$ DMRG simulations of the antiferromagnetic square-lattice Heisenberg model.

We further compare in Fig. S1(b, c) the pairing correlation obtained by both grand canonical and canonical finite-size simulations, respectively. For smaller M , the grand canonical simulation will first identify mean-field-like bulk orders, which correspond to a nearly flat pairing correlations at long distances. As M increases, the system can take into account more and more quantum fluctuations around the mean-field orders, such that the pairing correlations scales down with M and established a power-law decay with an exponent around 0.62, indicating a quasi-long-range SC order for the 6-leg ladder systems. For the canonical DMRG calculation using a fixed particle number (Fig. S1(c)), the SC pairing correlations at longer distances are being suppressed for small M , and larger M is required for their development. Thus the pairing correlations scale up with M , which also reach a very similar power-law decay with an exponent around 0.55 by extrapolation to infinite M limit. The similar exponents obtained by both grand canonical and canonical DMRGs demonstrate the equivalence of the two methods and the good convergence reached for $L_y = 6$ systems. For $L_y = 8$ systems, we obtain reliable results for bulk order and qualitatively accurate behavior for pairing correlations. However quantitatively, it is very difficult to obtain accurate long-distance correlations with finite bond dimensions accessible by current computational power, and much larger bond dimensions are needed to obtain accurate power-law exponent specific for the quasi-1D 8-leg systems. Thus for a large system, grand canonical DMRG is a proper way to detect ground state SC orders, approximating physics in the thermodynamic limit as long as such orders are robust with the increase of the bond dimensions and system sizes.

Appendix B: DMRG convergence

Most of the results presented in the main text are obtained for a system size of $N = 50 \times 8$, and we keep bond dimension upto $M = 15000$, which gives a truncation error smaller or around 3.0×10^{-5} . We show in Fig. S2(a) and (b) the scaling of the ground state energies in terms of the bond dimension for both $L_y = 6$ and 8 , which gives the energy density $E/N = -6.590$ and -6.593 , respectively. The closeness between energy densities at the largest bond dimension and those extrapolated to infinite M for both systems demonstrate a good convergence of the ground state.

In Fig. S2(c) and (d), we compare the non-local pairing orders on a six-leg system by both $SU(2)$ and $U(1)$ simulations with $m = M = 10000$, and find quantitative agreement between them, indicating a robust structure of the Cooper pair insensitive to the bond dimension or spin symmetry imposed in our simulations.

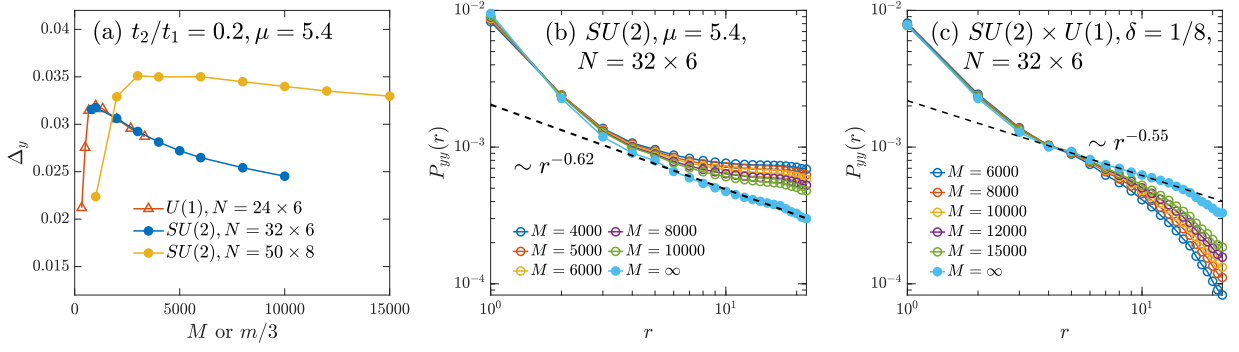


FIG. S1. (a) $t_2/t_1 = 0.2$ and $\mu = 5.4$. The change of bulk pairing order parameters with the bond dimensions. The $SU(2)$ bond dimension M is counting the number of spin $SU(2)$ multiplets, which corresponds to about 3 times of the $U(1)$ bond dimension m . Both six-leg and eight-leg systems are studied, and the latter show larger SC orders and more robust plateau for Δ_y with respect to M , indicating SC in the thermodynamic limit. (b) Pairing correlations $P_{yy}(r)$ at different M s obtained by spin $SU(2)$ DMRG for grand canonical systems at fixed $\mu = 5.4$ for $t_2/t_1 = 0.2$ and $N = 32 \times 6$. A scaling to infinite M renders a power-law decay with an exponent around 0.62. (c) $P_{yy}(r)$ of a canonical system at doping $\delta = 1/8$ and $N = 32 \times 6$, with the power-law exponent around 0.55 for infinite- M extrapolated data.

Appendix C: Pairing Correlations and Charge-Bond Order in the Pure t - J Model

In the main text, we showed the pattern of the PDW order and its coupling with a spin-bond order. Here we present additional information on pairing correlations and charge bond order in the SC-PDW phase. The pairing correlation P_{yy} for the pure t - J model is nearly flat in the middle range in Fig. S3(a) and (b), reflecting the near long-range SC order. The strong-weak alternation in its magnitude along \hat{y} is also exhibited by comparing pairing correlations for $y = 1, 2$ in (a) and (b), respectively. In the inset of (b), we show the mean values of $P_{yy}(x, y = 2)$ in the middle 10 sites of the system for different M , which decays with the increase of M , indicating a reduced PDW order in the infinite M limit. A weak alternation of charge bond order along \hat{y} is similar to the strong-weak unit-2 pattern of PDW and spin-bond order in Fig. 4(c) and (d) in the main text, indicating additional intertwining between SC, spin and charge orders.

Appendix D: The Spatial Range of Cooper Pairs and The Exponential Decay of Correlations in the Hole- and Electron-Doped t - J Models

In the main text, we showed various correlations for the pure t - J model. Here we present additional results in the presence of a small t_2 . The long-distance pairing $\tilde{\Delta}(r) = \langle \hat{c}_\uparrow(\mathbf{r}_0) \hat{c}_\downarrow(\mathbf{r}_0 + r\mathbf{e}_x) - \hat{c}_\downarrow(\mathbf{r}_0) \hat{c}_\uparrow(\mathbf{r}_0 + r\mathbf{e}_x) \rangle / \sqrt{2}$, single-particle Green's function $G(r) = \langle \sum_\sigma \hat{c}_\sigma^\dagger(x, y) \hat{c}_\sigma(x + r, y) \rangle$, charge density correlation $D(r) = \langle \hat{n}(x, y) \hat{n}(x + r, y) \rangle - \langle \hat{n}(x, y) \rangle \langle \hat{n}(x + r, y) \rangle$ and spin correlation $S(r) = \langle \hat{\mathbf{S}}(x, y) \cdot \hat{\mathbf{S}}(x + r, y) \rangle$ can all be described by exponential decays with very short correlation lengths (see Fig. S4). Antiferromagnetic spin patterns are observed in Fig. S4 (a3) and (b3), and the short-range spin correlations are consistent with a short-range RVB spin background, driven by the frustrating NN hopping.

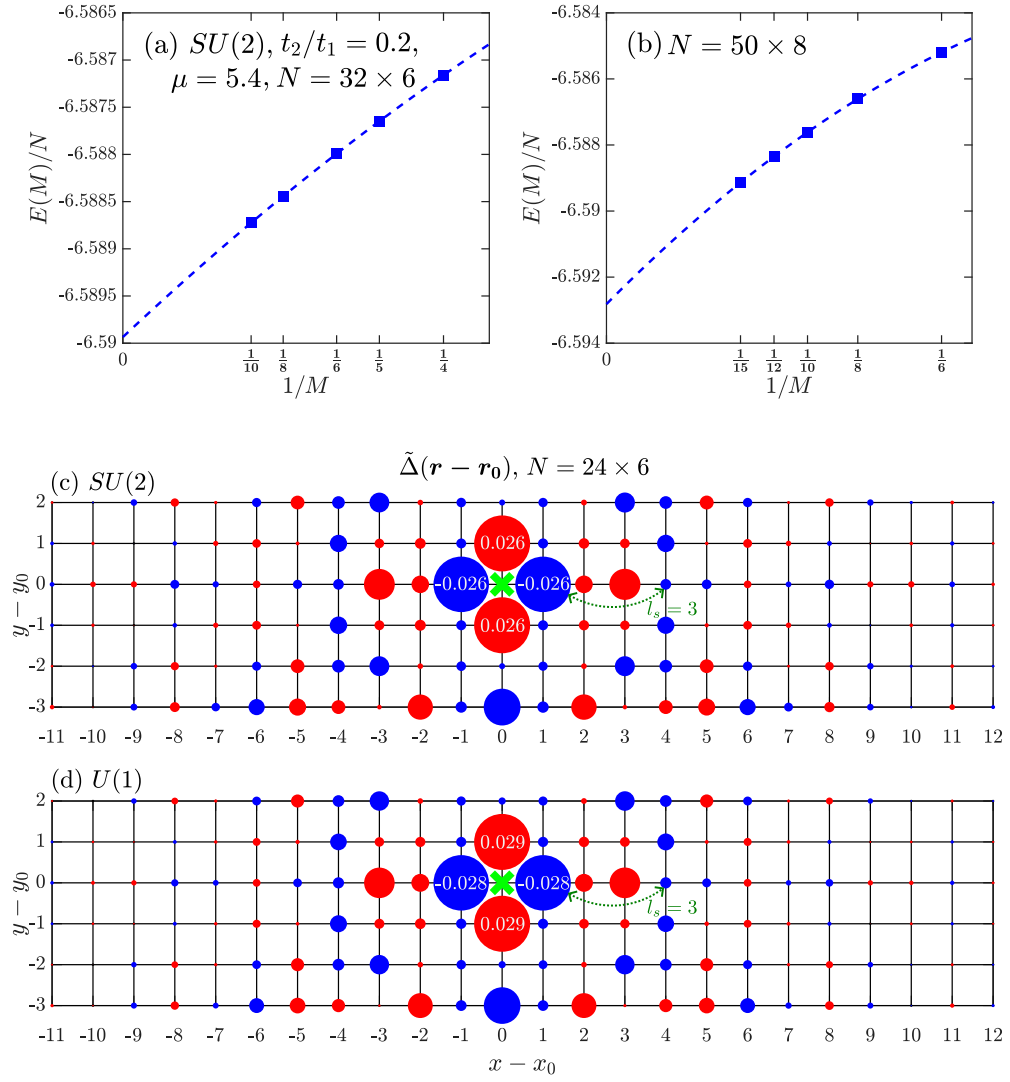


FIG. S2. $t_2/t_1 = 0.2$, $\mu = 5.4$. (a) Ground-state energy extrapolation to infinite M for $N = 32 \times 6$ with extrapolated energy $E(M \rightarrow \infty)/N = -6.590$. (b) Similar to (a) for $N = 50 \times 8$ with $E(M \rightarrow \infty)/N = -6.593$. (c) and (d) are non-local pairings $\tilde{\Delta}(\mathbf{r} - \mathbf{r}_0)$ imaging Cooper pairs for $N = 24 \times 6$ obtained by spin $SU(2)$ (with $M = 10000$) and spin $U(1)$ (with $m = 10000$) DMRG simulations respectively, which are quantitatively similar.

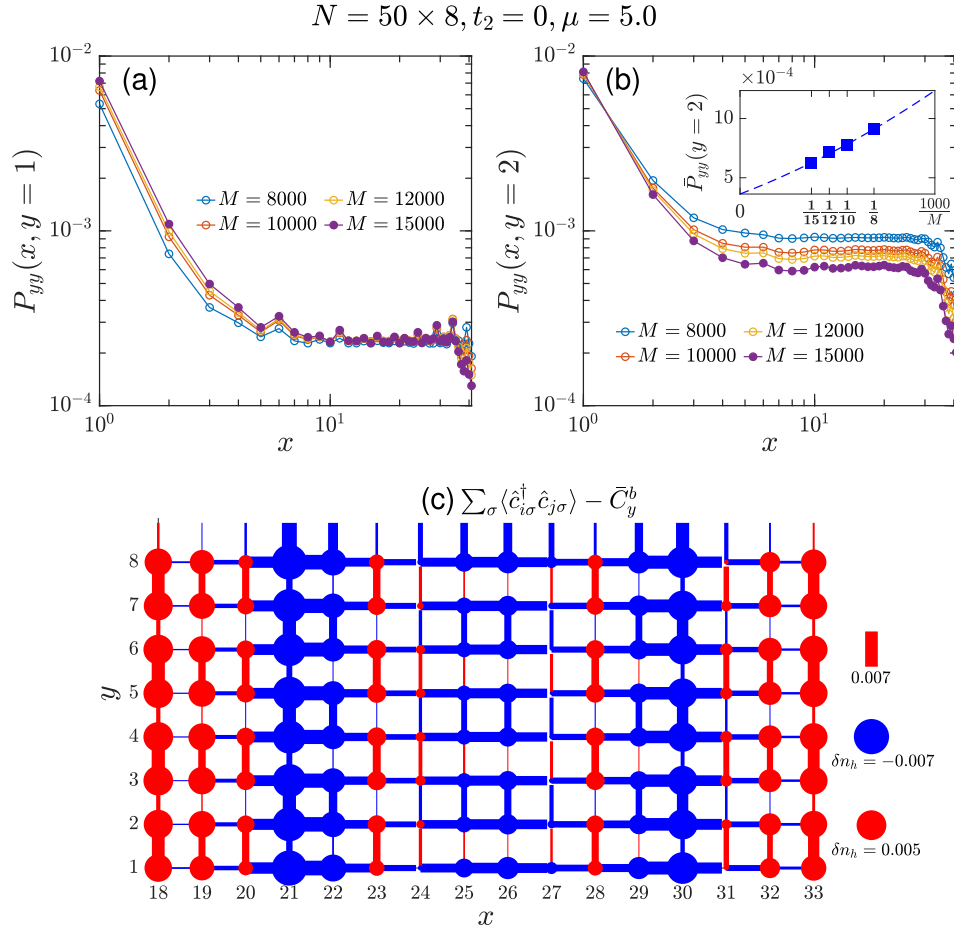


FIG. S3. $N = 50 \times 8, t_2/t_1 = 0$ and $\mu = 5.0$. (a-b) Pairing correlations $P_{yy}(x, y)$ for $y = 1, 2$ at different bond dimensions. In the inset of (b), we show the mean values of $P_{yy}(x, y = 2)$ in the middle 10 sites of the system for different M , and extrapolate them to infinite M limit. (c) Nearest-neighbor charge bond orders $\sum_{\sigma} \langle \hat{c}_{i\sigma}^{\dagger} \hat{c}_{j\sigma} \rangle - \bar{C}_y^b$ and hole density variations $\delta n_h(\mathbf{r}) \equiv n_h(\mathbf{r}) - \bar{n}_h$ obtained under $M = 12000$, with the subtracted mean values $\bar{C}_y^b \equiv \sum_i \sum_{\sigma} \langle \hat{c}_{i\sigma}^{\dagger} \hat{c}_{i+e_y, \sigma} \rangle / N_c = 0.095$ and $\bar{n}_h = \sum_i n_h(i) / N_c = 0.134$, where N_c is the number of sites in the figure.

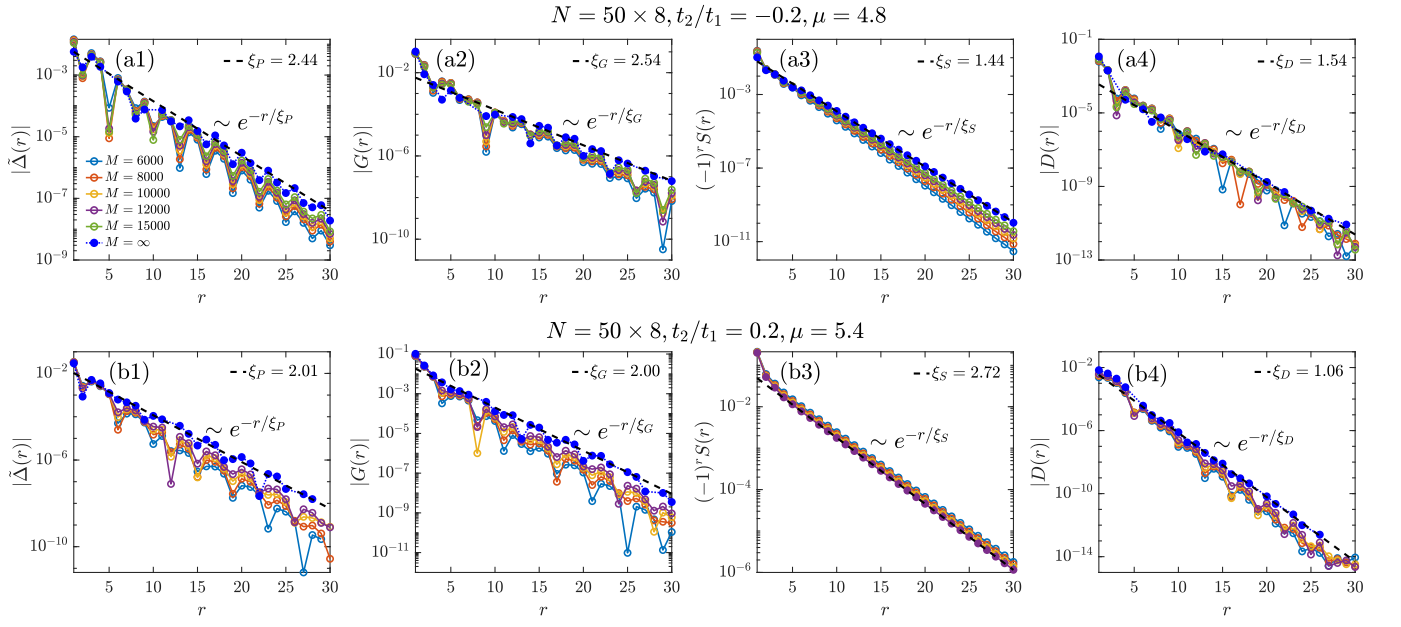


FIG. S4. (a1-a4) Non-local pairing $\tilde{\Delta}(r)$, single-particle Green's function $G(r)$, antiferromagnetic spin correlation $(-1)^r S(r)$ and density-density correlation $D(r)$ for $t_2/t_1 = -0.2$ obtained at different bond dimension M s and their extrapolations to infinite M , which are then fitted by exponential decays. (b1-b4) are similar plots for $t_2/t_1 = 0.2, \mu = 5.4$ and $N = 50 \times 8$.